Supporting Information

Raatikainen et al. 10.1073/pnas.1219591110

SI Text

Description of Data Sets Considered in this Study. Experimental data sets, which are all acquired by the Droplet Measurement Technologies Cloud Condensation Nuclei (CCN) counters (1, 2), are summarized in Table 1, and their geographical distributions are shown in Fig. 2. The analysis focuses on published high-quality data sets where threshold droplet growth analysis (TDGA) could not rule out the presence of kinetically limited droplets. Careful filtering of pressure and supersaturation transients, noting the instrument and model accuracy limits, and accounting for possible instrument operation issues are critical for unbiased conclusions on droplet growth kinetics. The data sets are fully presented in other publications; only brief overviews focusing on the model inputs (instrument operation parameters, calibrated supersaturation, dry particle size distribution, and hygroscopicity defined by the κ parameter; ref. 3) are given below.

International Consortium for Atmospheric Research on Transport and Transformation 2004. As a part of the International Consortium for Atmospheric Research on Transport and Transformation (ICARTT), the New England Air Quality Study–Intercontinental Transport and Chemical Transformation (NEAQS-ITCT) (4) took place in the northeastern United States during the summer of 2004. High aerosol concentrations are common in this industrialized and densely populated region due to both local and distant sources (5). Our analysis is focused on CCN measurements at the University of New Hampshire measurement site Thompson Farm in Durham, NH. Although local aerosol sources are not important for this rural site, elevated aerosol concentrations are observed when air masses originate from the more polluted south–west sector (6, 7). On the other hand, aerosol concentrations are significantly lower when air masses originate from the North Atlantic.

The Thompson Farm campaign was the first field deployment of the Droplet Measurement Technologies CCN instrument, and that first-generation instrument had some hardware issues with temperature and water flow controls. These issues were more common in the early part of the campaign, so we focus here on the time period from July 31 to August 11. Details about the measurements are given in ref. 8. Briefly, the CCN counter was operated at a stepping supersaturation mode (five steps between 0.1% and 0.6%) while sampling total CN, i.e., no other size selection in addition to a 2.5-μm cyclone was used. Dry particle size distributions between 7 and 300 nm were measured by a scanning mobility particle sizer (SMPS). Size distribution measurements took typically 135 s; therefore, CCN data were averaged for each SMPS scan. For the current analysis, dry particle hygroscopicity described by κ (9) is calculated from the size distributions and measured CCN concentrations. Assuming that all particles in a size distribution have the same κ, there is a single critical dry size so that all particles larger than this are activated at a fixed instrument supersaturation. This number of activated particles is known from the CCN measurements, so the critical dry size can be calculated and further converted to κ. Model simulations are based on measured size distributions (103 size bins spanning 7–300 nm). All particles in a size distribution have the same κ calculated from the instrument supersaturation and the characteristic dry particle diameter required to obtain closure between CCN concentration and the integrated size distribution.

European Integrated Project on Aerosol Cloud Climate and Air Quality Interactions 2007. The European Integrated Project on Aerosol Cloud Climate and Air Quality Interactions (EUCAARI; ref. 10) campaign took place in Hyytiälä, Finland, between March and May 2007. The Hyytiälä measurement station is located at a rural area surrounded mostly by Boreal forests (10). When air masses originate from the North Atlantic or Arctic Ocean, aerosol mass concentrations are generally low and dominated by organics possibly from biogenic sources (11, 12). The station also receives more polluted and aged air masses from central Europe and Russia. TDGA has been used to study CCN activation and growth kinetics (13). Average ambient droplet size at the activation supersaturation was similar to that for the calibration aerosol, but exhibited about 1-μm (20%) variations, which could indicate nonnegligible changes in droplet growth kinetics. In addition, droplet size distributions were sometimes bimodal over a range of instrument supersaturation, possibly indicating large differences in droplet growth kinetics. Therefore, this is a good data set for a more detailed analysis.

As described in ref. 13, CCN measurements were conducted by stepping both supersaturation (eight steps between 0.1% and 2%) and dry particle size (20, 40, 60, 80, and 100 nm, but the 20- and 100-nm data were not considered). A full cycle took about 30 min, resulting in an activation spectrum (CCN/CN as a function of supersaturation, where CN is condensation nuclei concentration) for each dry size. A sigmoidal function was fitted to the activation spectra to find the asymptotic maximum fraction of particles that can be activated and the characteristic (median) activation supersaturation, which was converted to characteristic hygroscopicity (13). Model simulations are based on the average particle properties described by the centroid mobility diameter, hygroscopicity, and measured CN concentration multiplied by the maximum activated fraction. The CN concentration scaling is needed to correctly simulate CCN concentrations, which determine the water vapor depletion effects (14).

Megacities Impacts on Regional and Global Environments 2006. As a part of the Megacity Initiative: Local and Global Research Observations (MILAGRO) program, the Megacities Impacts on Regional and Global Environments (MIRAGE)–Mexico took place in Mexico City, Mexico, during March 2006 (15). High aerosol concentrations are common due to significant anthropogenic emissions, meteorological conditions, and local topography. Unlike in Hyytiälä where anthropogenic biomass burning and vehicle emissions are rarely seen (12, 16), these are the main organic aerosol components in Mexico City (17, 18). The high secondary organic aerosol concentrations are related to the location of the city at a plateau 2,240 m above sea level surrounded by mountain ranges from three directions. The high altitude means enhanced photochemistry, and the mountains limit the dilution and transport of aerosol pollution. Padró et al. (19) have studied growth kinetics of the water-soluble fraction of Mexico City aerosol by applying TDGA to an offline CCN data set using filter samples collected during the MILAGRO campaign. Even though they did not see kinetic limitations in their 12-h average data, we will analyze another high-resolution on-site data set (20) to see if the same conclusions hold.

The on-site Droplet Measurement Technologies CCN instrument was operating at the T1 surface site (Universidad Tecnológica de Tecámac) about 30 km NNW from the urban T0 site (20). The instrument operation setup was similar to that used in Hyytiälä: nine supersaturation steps (0.1–1.2%) were taken during the 30-min cycle, and four (40, 60, 80, and 100 nm) dry particle sizes were sampled during each supersaturation step. Again, a sigmoidal function was fitted to each activation spectrum resulting in the maximum activated fraction and the characteristic activation supersaturation, which was converted to hygroscopicity. Model inputs are similar to those in Hyytiälä.

August Mini-Intensive Gas and Aerosol Study 2008. The August Mini-Intensive Gas and Aerosol Study (AMIGAS) took place in downtown Atlanta, GA. High aerosol concentrations are common in Atlanta, especially during the later summer months due to high sulfate and secondary organic aerosol (SOA) concentrations (21, 22). Unlike in many other urban areas such as Mexico City, a large fraction of the SOA is from regional biogenic sources (23–26). The AMIGAS campaign was therefore focused on examining the interactions between biogenic and anthropogenic volatile organic carbon (VOC) emissions and their contributions to SOA. Padró et al. (19) have examined droplet growth kinetics using the TDGA method. They found that observed droplet size was sometimes clearly below of that of the calibration aerosol by more than 1.0 μm. This droplet size difference was observed for elevated CCN concentrations and at larger supersaturations, possibly indicating water vapor depletion effects (14).

During the campaign, the Droplet Measurement Technologies CCN instrument was operated in scanning mobility CCN analysis (SMCA) mode (27), where a narrow dry particle size range is selected by a differential mobility analyzer (DMA) while continuously changing the DMA voltage. In this case, the voltage limits corresponded to a mobility diameter range from 7 to ~500 nm (19). Each up-scan took 120 s, and an additional 15 s were used to decrease the DMA voltage. Instrument supersaturation was changed after every 6 min so that five supersaturations from 0.2% to 1.0% were covered during the 30-min measurement cycle (19). Each mobility scan with a fixed supersaturation produced an activation spectrum with activation ratios (CCN/CN) as a function of dry particle size. The sigmoidal fits to the activation spectra gave the maximum activated fraction and characteristic activation dry particle size, which was converted to the characteristic hygroscopicity (19). Model simulations are based on the 1-s average particle properties described by the centroid mobility diameter, characteristic hygroscopicity, and CN concentration multiplied by the maximum activated fraction.

Gulf of Mexico Atmospheric Composition and Climate Study 2006. The Gulf of Mexico Atmospheric Composition and Climate Study (GoMACCS) and the Second Texas Air Quality Study (TexAQS II) were two simultaneous campaigns focused on air pollution around Houston, TX (28). TexAQS II focused on the health effects, whereas the GoMACCS focused on the climate effects including aerosol–cloud interactions (28). High aerosol and ozone concentrations are common in this densely populated and heavily industrialized region containing several oil refineries (29). Just like in Atlanta, most of the aerosol mass is sulfate and organics, but the biogenic contribution to SOA seems to be lower (30). We focus on the CCN measurements made on board the Center for Interdisciplinary Remotely Piloted Aircraft Studies (CIRPAS) Twin Otter research aircraft (31). Because these airborne CCN measurements were not size resolved, applicability of the TDGA method is limited by the fact that there is a range of activation supersaturations (and corresponding droplet sizes) to be compared against calibration aerosol. Therefore, Lance et al. (31) compared average ambient aerosol droplet sizes to those of ammonium sulfate aerosol with dry size from 10 to 200 nm. Ambient aerosol droplet size was generally larger than that of the calibration aerosol indicating fast growth kinetics, but significant droplet size variations up to 2 μm (up to 50% of the mean droplet size) were observed. Such variations could indicate significant changes in droplet growth kinetics.

From the 17 flights with CCN data, there were four flights (7, 11, 16, and 17) where instrument supersaturation was stepped between three values (0.3–1.0%), and it was kept constant (0.3–0.7%) during the other flights (31). Each dry particle size distribution measurement by a dual automated classified aerosol detector (DACAD; ref. 32) took 73 s, so the CCN data were averaged to the DACAD time resolution. Measurements where the CCN counter was connected to another sample line containing cloud droplet residuals (sampled with a Counterflow Virtual Impactor) were ignored, because size distributions were always measured from the main sample line. Dry particle hygroscopicity (κ) was calculated from the dry size distributions and measured CCN concentrations using the same method as with the ICARTT data. Model inputs are also similarly based on the measured dry particle size distributions (85 size bins from 10 to 800 nm) and a constant κ for each distribution.

Aerosol, Radiation, and Cloud Processes Affecting Arctic Climate 2008. The Aerosol, Radiation, and Cloud Processes Affecting Arctic Climate (ARCPAC) was an airborne measurement campaign focusing on Arctic aerosol around Alaska during spring 2008 (33). Because local aerosol sources are scarce in the Arctic region, long-range transport from mid-latitudes together with slow removal processes during the winter leads to an accumulation of aerosol pollution, which is commonly known as the Arctic haze (34–36). Most of the air pollution in the Alaskan Arctic originates from Asia and Europe with a smaller contribution from North American continent and the surrounding oceans (37–40). Background haze, biomass burning plumes, and anthropogenic pollution were also encountered during the ARCPAC campaign (33).

There were five research flights in the Alaskan Arctic with a Droplet Measurement Technologies CCN instrument on board (41). Instrument operation mode was similar to that during the GoMACCS campaign, i.e., supersaturation was changed stepwise between one and three values (0.1–0.6%) while sampling particles without size selection. When CCN concentrations needed about 1 min to reach an equilibrium value after a supersaturation change (41), this was not enough for the droplet size. As a result of these transients, each supersaturation step was averaged to include about 40–60 s of data from the end of the step. High time resolution (1 s) dry particle size distributions were measured by an ultra-high sensitivity aerosol size spectrometer (UHSAS) and a nucleation mode aerosol size spectrometer (NMASS) (41), but these were averaged for the CCN data time sections. Dry particle hygroscopicity was calculated from the averaged dry size distributions and CCN concentrations using the same method as in the GoMACCS data analysis. Similarly, the model simulations are based on the measured dry particle size distributions (118 size bins from 5 to 975 nm) and a constant κ for each distribution.

Arctic Research of the Composition of the Troposphere from Aircraft and Satellites 2008. The National Aeronautics and Space Administration (NASA) Arctic Research of the Composition of the Troposphere from Aircraft and Satellites (ARCTAS) summer campaign (ARCTAS-B) was another airborne campaign focusing on Arctic aerosol and especially fresh and aged fire plumes (42), which are known to have a significant contribution to Arctic aerosol mass concentrations (37, 38). From the three research aircraft used in the ARCTAS campaign, we focus on the DC-8, which was equipped with a Droplet Measurement Technologies CCN counter. The flights covered large areas over Canada and Greenland (Denmark), including a flight to the high Arctic near 90° N, and transit flights to and from Los Angeles, CA. Several flights were focused on local forest fire plumes near Cold Lake, Canada, but also anthropogenic pollution and long-range transported fire plumes from Siberia were encountered (42).

Details of the CCN measurements, which were similar to those during the ARCPAC campaign, are given in Lathem et al. (43). The transit flight to Canada and the first flight there had to be discarded due to instrumental issues, so here we focus on flights 18–24 from July 1–14, 2008. Instrument supersaturation was stepped between two or three values ranging from 0.2% to 0.9%. Dry particle size distributions (8.5–414 nm) were measured by an SMPS and merged with distributions obtained with an UHSAS, providing a composite distribution ranging from 8.5 nm to 1 μm. The CCN data were averaged over the 105-s SMPS time resolution. Aerosol hygroscopicity was calculated initially from the dry size distributions and CCN concentrations, but these proved

to be noisy. Therefore, hygroscopicity was estimated from chemical composition data measured by a high-resolution time-of-flight aerosol mass spectrometer.

California Nexus 2010. The California Nexus (CalNex) campaign, which focused on climate change and air quality, took place in Los Angeles, CA, during summer 2010. High aerosol concentrations and other air quality issues are common in this densely populated and industrialized area (44). Typically about half of the aerosol mass is organics, and the inorganic fraction is mainly ammonium, nitrate, and sulfate including smaller sea salt and dust components (44–47). Aerosol composition and concentrations depend strongly on local meteorological conditions (e.g., wind direction) and the different geographical features such as the Pacific Ocean, the Los Angeles basin, and Sierra Nevada mountains affecting large scale air flows.

Most of the CalNex CCN data were recorded using the scanning flow mode (48), the kinetics interpretation of which requires a transient inversion analysis. The constant flow mode CCN data were collected during three flights with the CIRPAS Twin Otter aircraft (49) and two flights with the NOAA WP-3D aircraft (50). One NOAA WP-3D flight was an excursion to the Gulf of Mexico to examine the effect of the Deepwater Horizon oil spill on SOA, but this data set has already been analyzed by the model (50). The other NOAA WP-3D flight encountered problems in measuring dry particle size distributions. In addition, a steplike change in the droplet size was observed during one Twin Otter research flight, which was most likely caused by an obstruction in the instrument optics, so this flight was also discarded. The measurements during the two remaining flights are similar to those used in the other airborne campaigns discussed above and in Ensberg et al. (49). Constant supersaturation (0.31–0.34%) was maintained while sampling total aerosol. Dry particle size distributions (8–1,002 nm) were measured by a SMPS, and this limits the time resolution to 90 s. Aerosol hygroscopicity was calculated from dry particle size distributions and measured CCN concentrations.

Other studies cited but already analyzed in the literature. In addition to the eight data sets mentioned before, we also consider the kinetic analysis of two data sets: one obtained in the Eastern Mediterranean during the 2007 Finokalia Aerosol Measurement Experiment (FAME-07; refs. 51 and 52) and one during the 2010 airborne survey of airmasses in the vicinity of the BP Deepwater Horizon Oil spill (50). We also consider two studies focused on secondary organic aerosol produced from oxidation of biogenic hydrocarbons of global relevance (53, 54).

In the FAME-07 studies, measurements of total (51) and size-resolved (52) CCN concentrations between 0.2% and 1.0% supersaturation, aerosol size distribution and chemical composition were performed at the remote Finokalia site (35°32′ N, 25° 67′ E; http://finokalia.chemistry.uoc.gr) of the University of Crete in the eastern Mediterranean from July to October 2007. Most of the particles activate at <0.6% supersaturation, reflecting the aged nature of the aerosol in this region. Using threshold droplet growth analysis, the growth kinetics of CCN is consistent with rapid activation (NaCl calibration aerosol); hence, $\alpha_c = 0.2$ can be assumed for CCN activation in this region.

The Deepwater Horizon oil spill study sampled secondary organic aerosol from the oxidation of hydrocarbons emitted in the vicinity of the spill during two survey flights with the National Oceanic and Atmospheric Administration WP-3D aircraft in June 2010. Owing to the large CCN concentrations in the air masses sampled, TDGA could not exclude the presence of slowly activating CCN. The approach of Raatikainen et al. (55) was therefore used to comprehensively account for water vapor depletion effects on activated droplet size measured by the CCN instrument. The ability to capture the observed droplet size variability while assuming rapid activation ($\alpha_c = 0.2$) is shown in Fig. 4 and Moore et al. (50); failure to account for water vapor depletion effects leads to fluctuations in droplet size outside of the 0.3-μm uncertainty limit, which TDGA would misidentify as slowly growing droplets (Fig. 4). Therefore, CCN activation in this environment is as rapid as calibration aerosol; hence, $\alpha_c = 0.2$ can be assumed.

Engelhart et al. (53, 54) measured the CCN activity of SOA from oxidation of monoterpenes and isoprene for a wide range of conditions. Using threshold droplet growth analysis, the growth kinetics of CCN is consistent with rapid activation (NaCl calibration aerosol); hence, $\alpha_c = 0.2$ can be assumed for CCN activation. This result is important, because it reflects the activation behavior of environments rich in biogenic SOA (e.g., boreal forests, Amazon).

Detailed Analysis of Data Sets. Because the previous TDGA studies have shown that most droplets grow as quickly as the ammonium sulfate calibration aerosol, correlation plots showing the observed droplet size as a function of simulated droplet size for a fixed $\alpha_c = 0.2$ (the previously determined optimal value for ammonium sulfate; ref. 55) is used to detect the presence of slow water uptake kinetics. Correlation plots are suitable where one-to-one or even linear correlation is not expected due to shifts in the optical particle counter (OPC) size calibrations; such sizing biases can be a few microns or less, depending on the cleanliness of the instrument optics and the precision of the manufacturer OPC calibration (55). Model simplifications necessary for accelerating calculations lead to overestimation of droplet size at high instrument supersaturations; this bias, however, is negligible for supersaturation less than 1.0% (55). The predictions also depend on the accuracy of the input parameters such as supersaturation and thermophysical properties (56). As a result of these experimental and modeling biases, the correlation plots will show whether most data points will be focused around a monotonic curve. Deviations from this curve that are larger than the approximated 0.3-μm noise can indicate detectable changes in ambient aerosol water uptake coefficient. To simplify the comparison, a suitable polynomial function is fitted to each data set to represent fast kinetics; this is required to quantify the observation-prediction bias for the $\alpha_c = 0.2$ simulation and the 0.3-μm "noise" limits required for producing the probability distribution of data that deviate from the average (rapid) kinetics (Fig. 4).

Calibration experiments give an estimate of the smallest statistically significant change in α_c and droplet size. Optimal α_c for the calibration aerosol is 0.2, but this is practically indistinguishable from any α_c between 0.1 and 1.0 (55). This α_c range represents about ±0.3-μm droplet size uncertainty, which is a reasonable estimate for the noise during steady instrument operation and twice the theoretical range (α_c between 0.2 and 1.0) calculated by Miles et al. (56) for CCN measurement conditions similar to ours. We adopt the larger uncertainty range as it better reflects the uncertainty from instrument operation, especially given that varying α_c between 0.1 and 0.2 is not important for climate. Lowest detectable α_c depends on dry particle size, hygroscopicity, and instrument supersaturation, but generally values less than 0.001 mean that droplets do not reach the 1-μm droplet detection limit of the CCN instrument. As a result, slowly growing droplets with α_c from 0.1 to 0.001, which have at least 0.3-μm effect on the droplet size, can be distinguished from the rapid growth with $\alpha_c = 0.2$.

ICARTT 2004. A first inspection of the data shows that there are at least six instances in which the correlation between observed and simulated droplet sizes changes abruptly. These changes can be related to two types of instrument issues. First, instrument flooding and drying seem to have left residues to the OPC optics, and this has changed sizing slightly. Second, failures of the thermo-electric coolers (TECs) controlling the CCN chamber temperature gradient seem to have produced bimodal droplet size distributions, which have a large supersaturation dependent effect on the average droplet size. The bimodal droplet size distributions can be explained by the fact that even a small local perturbation

in the CCN chamber wall temperature profile can produce a dip to the otherwise slowly increasing centerline supersaturation profile resulting in two maximum supersaturation values. When an aerosol distribution reaches the first lower maximum, the largest and more hygroscopic particles activate. Slightly smaller and less hygroscopic particles activate at the second larger maximum, and because of the different growth times, the final droplet size distribution is split.

For clarity, Fig. S1*A* shows only the two most different sections of the data. Marker color is based on instrument supersaturation being approximately 0.2%, 0.3%, 0.37%, 0.5%, and 0.6%. Quadratic polynomials have been fitted to both sections to represent fast kinetics (solid lines) and to show the ±0.3-μm noise limits (dashed lines). The correlation between the observed and simulated droplet size is practically linear for the August 4–6 section, but the other section is clearly different due to a TEC failure, which produces bimodal droplet size distributions. The correlation is nonlinear, because the fraction of smaller droplets depends on instrument supersaturation being highest for the intermediate supersaturations. For example, typically droplets are larger than 1.5 μm at the 0.37% supersaturation, but here about one-third of the droplets were smaller. The only points that exceed the ±0.3-μm noise limits are seen in the series affected by a TEC failure. The deviations are also small, with both positive and negative deviations indicating increased noise. Therefore, we can conclude that the model can explain observed droplet size variability using a constant water vapor uptake coefficient; thus, ambient droplets grow as quickly as ammonium sulfate calibration aerosol. This conclusion is valid for the other sections that are not shown here.

The largest variations in the observed droplet size were about 1 μm, and additional simulations showed that these are mainly caused by water vapor depletion effects (14). This simulation result is in good agreement with expectations, because CCN concentrations often exceeded 1,500 cm^{-3} (ambient pressure). The effects of hygroscopicity and dry particle size variations on droplet size were much smaller, but this is largely caused by uncertainties in hygroscopicity and lack of knowledge of the 300- to 2,500-nm dry particle size distributions. Examples of the filtering applied for the droplet kinetic analysis is provided in Fig. S2.

EUCAARI 2007. Fig. S1*B* shows the correlation between observed and simulated droplet sizes. Dry particle sizes are indicated by different marker colors, and different supersaturations can be seen as partly overlapping data clusters. The lowest supersaturations (<0.6%) and those that are not at least 0.2% larger than the characteristic activation supersaturation were filtered to reduce biases due to insufficiently precise characterization of particle size or hygroscopicity distributions. Simulated and observed droplet sizes are generally very similar in magnitude, and the deviations from the ideal one-to-one correlation are well within the normal instrument sizing and simulation uncertainties. A quadratic polynomial was fitted to the data to represent fast kinetics (solid line) and to calculate the ±0.3-μm noise limits (dashed lines). Most of the data points are within the noise limits, and a detailed inspection of the outliers showed that the largest (>1 μm) deviations occur right after column top temperature changes, so they are caused by instrument transients. However, some of the smaller (~0.5 μm) deviations in the 40-nm data series are seen due to a secondary droplet mode similar to those observed in the ICARTT data above. Because this is also most likely an instrument bias (a TEC failure as discussed above), we conclude that the average droplets grow as quickly as the ammonium sulfate calibration aerosol, which is in good agreement with the previous TDGA study (31).

The largest variations in the observed droplet size were about 1.5 μm, and model simulations showed that these were mainly caused by variations in dry particle hygroscopicity. This finding shows the importance of accounting for hygroscopicity; if hygroscopicity variations were neglected, the observed 1.5-μm variations in droplet size would have been interpreted as significant changes in water uptake coefficient. The effect of dry particle size variations on droplet size was negligible due to the initial size selection. For the same reason, CCN concentrations were always less than 250 cm^{-3} and rarely exceeded 100 cm^{-3} (ambient pressure), resulting in negligible water vapor depletion effects.

MIRAGE 2006. Fig. S1*C* shows the correlation between observed and simulated droplet size for the four dry particle sizes. Again, supersaturations that are not at least 0.2% larger than the characteristic supersaturation were filtered due to the model limitations. A quadratic polynomial was fitted to the data to represent fast kinetics (solid line), and the ±0.3-μm noise limits (dashed lines) are also included. It seems that there is a dry size-dependent bias so that the model overpredicts droplet size for the 40-nm particles and underpredicts that for the 100-nm particles. Instead of differences in droplet growth kinetics, this seems to be related to a small bias in the droplet growth times caused by the model simplifications. If these dry sizes were considered separately, there would be very few outliers. However, this is not necessary because the variations in the combined case are also almost exclusively within the 0.3-μm uncertainty limits. A closer look at the clear outliers reveals that these are again related to instrument transients. Therefore, the conclusion is that the droplets grow as quickly as the ammonium sulfate calibration aerosol, which is in good agreement with the previous offline study (19).

Hygroscopicity variability is once more the main reason for droplet size variability, but this time water vapor depletion has an observable effect. For the highest CCN concentrations (1,000–2,000 cm^{-3} at ambient ~750 mbar pressure) and the largest droplet sizes, the model predicts an ~10% (0.7 μm) decrease in droplet size, which is clearly above the noise limit.

AMIGAS 2008. Simulation results are shown in Fig. S1*D*. For clarity, only the data for 140- to 160-nm dry sizes are shown, but the correlation would be similar for the other dry sizes. The 0.2% supersaturation data are not included, because average droplet size is often too close to the OPC detection limit (about 1 μm). The data are also filtered by removing possibly noisy data points with less than 25 particle counts [$\sigma(N)/N \geq 0.2$ when assuming Poisson counting statistics] and points where dry size is less than 30% larger than the characteristic dry size. The figure also shows a cubic function fitted to the data to represent fast kinetics and the typical ±0.3-μm uncertainty limits.

Most of the outliers exceeding the uncertainty limits are in a small cluster of 0.4% supersaturation data points that seem to have a larger (than average) simulated droplet size. Given that these particles are with relatively high κ (~0.6) and large CCN concentrations, a 10% undercounting of CCN (57) explains underpredicting supersaturation depletion effects and overpredicting droplet size. CCN size-dependent hygroscopicity causing a decrease in the observed droplet size with increasing dry size is the main explanation for the largest deviations for the three largest supersaturations. There are also a few scans (10–30 of 3,214) where some smaller droplets are observed. Unlike in Hyytiälä and Thomson Farm where clear bimodal droplet size distributions were observed, most of the smaller droplets are just single counts distributed evenly between the OPC detection limit and the main droplet mode. Theoretically, these droplets could have lower water uptake coefficients, but a smaller externally mixed particle mode activating after the main mode is another possible explanation. Because these droplets are a small fraction of total CCN and have a negligible effect on the average droplet size, significant kinetic limitations can be ruled out. This conclusion is in good agreement with the TDGA analysis by Padró et al. (57), except that they also rarely observed significantly smaller (>1.0 μm) droplets. Our filtering removed these points, so it is possible that the outliers in Padró et al. (57) are just noisy data points.

Most variations in the observed droplet size can be explained by both time- and size-dependent variations in dry particle hygroscopicity. Model simulations are based on time dependent hygroscopicity only, which means that they cannot fully capture the observed droplet size variability, but the simulations seem to be accurate most of the time. Measured CCN concentrations were always less than 600 cm^{-3} and generally less than 100 cm^{-3} (at instrument pressure ~940 mbar), so significant water vapor depletion effects were not expected, and this was confirmed by model simulations showing negligible changes in droplet sizes.

GoMACCS 2006. The first model runs show that there is a steplike change in the difference between observed and simulated droplet size. The difference was initially ~0.5 μm, but after flight 9 (August 29, 2006) it increased to ~1.0 μm. This increase seems to be related to the instrument pressure, which changed with altitude during the first nine flights, after which a Droplet Measurement Technologies inlet pressure controller was installed to keep it at about 700 mbar (31). To simplify the comparison, 0.5- (before pressure controller) and 1.0-μm (after pressure controller) corrections were applied to the observed droplet size. In addition to this constant bias, the first correlation plots showed that deviations were often larger than 2.0 μm. Most of these were clearly caused by transients seen after supersaturation, column top temperature, and pressure changes. Because it is not possible to filter all suspicious data points without also filtering possible cases with slow droplet growth kinetics, only the most obvious pressure variations (more than 15-mbar differences from next or previous pressure value) were removed. Examples of the filtering applied for the droplet kinetic analysis is provided in Fig. S2.

The pressure-filtered results for the 17 flights including a linear fit to the data to and the typical ±0.3-μm (and in this case, more realistic ±0.5-μm) uncertainty limits are shown in Fig. S1*E*. Labels are not shown due to the space limitations, but each of the 17 flights has a different marker color, and the two marker types indicate the constant and stepping supersaturation mode flights. A few points exceed the ±0.5-μm uncertainty limit, but the deviations are large (~1 μm) when this happens. A careful inspection of the raw data shows that additional transients (e.g., column top temperature and supersaturation) and changes in aerosol properties during the averaging time are likely explanations for the deviations. For example, transient supersaturations most likely cause the positive deviations for the stepping supersaturation flights (the circles above the linear fit), and the largest deviations during the constant supersaturation flights are seen when there are significant variations in CCN concentrations (possibly indicating changes in aerosol properties). Because transients or changes in CCN during the 73-s averaging time can explain the largest differences between observed and simulated droplet sizes, fast kinetics can be assumed for the whole data set.

CCN concentrations were generally high and sometimes exceeded 10,000 cm^{-3} (at ambient pressure), which should cause clear water vapor depletion effects (14). The simulations showed that water vapor deletion could have up to a 15% (1 μm) effect on average droplet size. This effect was also seen in the experimental data, although CCN concentration variations within the 73-s averaging time also contributed to droplet size variability. The effects of hygroscopicity and dry particle size on droplet size are not as clear as in the size resolved data sets.

ARCPAC 2008. ARCPAC is another airborne campaign in which the stepping supersaturation mode was used, so increased droplet size variability can be expected. On the other hand, pressure and flow rate fluctuations were lower than those during the GoMACCS campaign, and the clear transients were filtered before model simulations. In fact, this initial filtering was so effective that additional filtering is not needed. The ARCPAC results and a quadratic polynomial fitted to the data are shown in Fig. S1*F*. The observed droplet size is about 30% smaller than the simulated droplet size, but this is still within the experimental and modeling uncertainties. When this size bias is neglected, the difference between observed and predicted droplet size is mostly within the ±0.3-μm uncertainty limits. Again, a closer look at the raw data shows that transients and uncertainties in hygroscopicity can explain the largest deviations. Therefore, we can conclude that the droplet growth is as fast as that of the calibration aerosol. Examples of the filtering applied for the droplet kinetic analysis is provided in Fig. S2.

Variations in hygroscopicity can explain most of the relatively small changes in the average droplet size. Dry particle size distributions and water vapor depletion have a minor effect on droplet size. Model simulations showed that, for the largest CCN concentrations (less than 1,000 cm^{-3} at instrument pressure ~450 mbar), the change in droplet size due to water vapor depletion is just 0.1 μm, which is well below noise.

ARCTAS 2008. The ARCTAS data set and the results in Fig. S1*G* are similar to those from the ARCPAC campaign. Because ARCTAS data were not as strictly filtered for transients (compared with ARCPAC data), a slightly larger fraction of the data points exceeds the ±0.3-μm uncertainty limits. Small differences between the individual ARCTAS flights are also apparent. For example, most of the data points from the first flight (18) are below the quadratic fit line, but those from the last flight (24) are above the line. These differences, however, are much smaller than those in the GoMACCS campaign, where a 0.5-μm step was observed, so no correction is needed here. The largest differences between observed and simulated droplet sizes are generally less than 0.5 μm, which seems to be a better noise estimate for most airborne measurements. Therefore, fast kinetics can be assumed for this data set.

The effects of hygroscopicity and size distributions on droplet size are mostly within noise. The highest CCN concentrations during flights 18, 19, and 24 were regularly above 10,000 cm^{-3} (standard temperature and pressure), so significant water vapor depletion effects can be expected. In good agreement with the observations, model simulations showed that vapor depletion had up to a 25% (2 μm) effect on droplet size, which is well above noise.

CalNex 2010. CalNex data are practically free of transients due to the constant supersaturation and an effective pressure control. In addition, compared with those from the previous airborne campaigns, CCN concentrations are smooth, indicating well-mixed air masses, which yields averages with small variability. The results including a linear fit and ±0.3-μm uncertainty limits are shown in Fig. S1*H*. Only a few data points exceed the ±0.3-μm uncertainty limits, and the largest deviations are positive, which cannot be caused by kinetic limitations. Therefore, fast droplet growth kinetics can be concluded.

Because the largest CCN concentrations are 3,000 cm^{-3} (standard temperature and pressure), water vapor depletion has a small effect on droplet size (14). The simulations show that the largest decrease in droplet size is about 5% (0.3 μm), which is observable due to the low noise. For example, Pearson's correlation coefficient (R) for the observed and predicted droplet size (the linear fit in Fig. S1*H*) increased from 0.79 to 0.90 when the simulations account for water vapor depletion. The effect of hygroscopicity on droplet size is also observable, but size distribution effects are small.

Contrasting These Results Against Other Published Literature That Cite Low α_c. Careful filtering of pressure and supersaturation transients, noting the instrument and model accuracy limits (especially when supersaturation depletion occurs), and observing possible instrument malfunctions are critical for correct interpretation of droplet activation kinetics data from CCN measurements. Studies published to date may have been less aware of these issues and their importance, with implications for the kinetics

interpretation. Using TDGA, Asa-Awuku et al. (58) reported that 60% of the ambient average droplet sizes during the 2006 Texas Air Quality Study (which overlapped with the GoMACCS campaign) were smaller than the rapid activation standard. Slow droplet growth kinetics, however, is an unlikely explanation. Instead, water vapor depletion effects are likely due to the high CCN concentrations sampled combined with insufficient filtering of data against supersaturation transients, pressure fluctuations, and electronic (likely thermal) noise. Ruehl et al. (59) have also studied aerosol growth kinetics in Houston, TX. Their analysis suggested that about 25% of ambient particles experienced some degree of kinetic limitations. However, the variability in particle hygroscopicity distributions and effects of water vapor depletion could have explained some smaller droplet sizes. While studying droplet growth kinetics close to the California coast, Ruehl et al. (60) observed bimodal droplet size distributions from the activated CCN. This observation may be interpreted as a small subset of aerosol experiencing retarded activation kinetics; similar bimodal droplet size distributions caused by instrument operation problems, however, were observed in the ICARTT 2004 and EUCAARI 2007 data sets and could contribute to the small droplets observed in the study of Ruehl et al. (60). Finally, the chamber SOA study of Asa-Awuku et al. (61) detected the presence of slowly growing CCN produced during the dark ozonolysis of β-caryophyllene. Although there was no evidence indicating that growth delays were caused by instrument issues or vapor depletion effects, subsequent studies attempting to reproduce this result were unsuccessful. Therefore, even if dark ozonolysis of β-caryophyllene leads to slowly growing particles, it occurs with limited frequency and is not overall a major contributor to global CCN.

Three-Dimensional Distributions of N_d from Global Model Simulations. Figs. S3 and S4 shows the average annual average droplet number concentration, N_d, at the 936-mb pressure level, for preindustrial and current day simulation, respectively. In all these figures, results are shown for $\alpha_c = 1.0$ (*Upper Left*), 10^{-1} (*Upper Right*), 10^{-2} (*Lower Left*), and 10^{-3} (*Lower Right*).

1. Roberts GC, Nenes A (2005) A continuous-flow streamwise thermal-gradient CCN chamber for atmospheric measurements. *Aerosol Sci Technol* 39(3):206–221.
2. Lance S, Medina J, Smith JN, Nenes A (2006) Mapping the operation of the DMT continuous flow CCN counter. *Aerosol Sci Technol* 40(4):242–254.
3. Petters MD, Kreidenweis SM (2007) A single parameter representation of hygroscopic growth and cloud condensation nucleus activity. *Atmos Chem Phys* 7(8):1961–1971.
4. Fehsenfeld FC, et al. (2006) International consortium for atmospheric research on transport and transformation (ICARTT): North America to Europe: Overview of the 2004 summer field study. *J Geophys Res* 111(D23):D23S01.
5. Rahn KA, Lowenthal DH (1985) Pollution aerosol in the northeast: Northeastern-midwestern contributions. *Science* 228(4697):275–284.
6. Slater JF, Dibb JE (2004) Relationships between surface and column aerosol radiative properties and air mass transport at a rural New England site. *J Geophys Res* 109 (D1):D01303.
7. Cottrell LD, et al. (2008) Submicron particles at Thompson Farm during ICARTT measured using aerosol mass spectrometry. *J Geophys Res* 113(D8):D08212.
8. Medina J, et al. (2007) Cloud condensation nuclei closure during the International Consortium for Atmospheric Research on Transport and Transformation 2004 campaign: Effects of size-resolved composition. *J Geophys Res* 112(D10):D10S31.
9. Kulmala M, et al. (2009) Introduction: European Integrated Project on Aerosol Cloud Climate and Air Quality interactions (EUCAARI): Integrating aerosol research from nano to global scales. *Atmos Chem Phys* 9(8):2825–2841.
10. Kulmala M, et al. (2001) Overview of the international project on biogenic aerosol formation in the boreal forest (BIOFOR). *Tellus B Chem Phys Meterol* 53(4): 324–343.
11. Allan JD, et al. (2006) Size and composition measurements of background aerosol and new particle growth in a Finnish forest during QUEST 2 using an aerodyne aerosol mass spectrometer. *Atmos Chem Phys* 6(2):315–327.
12. Raatikainen T, et al. (2010) Physicochemical properties and origin of organic groups detected in boreal forest using an aerosol mass spectrometer. *Atmos Chem Phys* 10(4):2063–2077.
13. Cerully KM, et al. (2011) Aerosol hygroscopicity and CCN activation kinetics in a boreal forest environment during the 2007 EUCAARI campaign. *Atmos Chem Phys* 11(23):12369–12386.
14. Lathem TL, Nenes A (2011) Water vapor depletion in the DMT continuous-flow ccn chamber: Effects on supersaturation and droplet growth. *Aerosol Sci Technol* 45(5): 604–615.
15. Molina LT, et al. (2010) An overview of the MILAGRO 2006 campaign: Mexico City emissions and their transport and transformation. *Atmos Chem Phys* 10(18):8697–8760.
16. Finessi E, et al. (2012) Determination of the biogenic secondary organic aerosol fraction in the boreal forest by NMR spectroscopy. *Atmos Chem Phys* 12(2):941–959.
17. Stone EA, et al. (2008) Source apportionment of fine organic aerosol in Mexico City during the MILAGRO experiment 2006. *Atmos Chem Phys* 8(5):1249–1259.
18. Aiken AC, et al. (2009) Mexico City aerosol analysis during MILAGRO using high resolution aerosol mass spectrometry at the urban supersite (T0)—Part 1: Fine particle composition and organic source apportionment. *Atmos Chem Phys* 9(17):6633–6653.
19. Padró LT, et al. (2010) vestigation of cloud condensation nuclei properties and droplet growth kinetics of the water-soluble aerosol fraction in Mexico City. *J Geophys Res* 115(D9):D09204.
20. Lance S, et al. (2012) Aerosol mixing-state, hygroscopic growth and cloud activation efficiency during MIRAGE 2006. *Atmos Chem Phys Discuss* 12(6):15709–15742.
21. Kim E, Hopke PK, Edgerton ES (2003) Source identification of atlanta aerosol by positive matrix factorization. *J Air Waste Manag Assoc* 53(6):731–739.
22. Butler AJ, Andrew MS, Russell AG (2003) Daily sampling of $PM_{2.5}$ in Atlanta: Results of the first year of the Assessment of Spatial Aerosol Composition in Atlanta study. *J Geophys Res* 108(D7):8415.
23. Lim H-J, Turpin BJ (2002) Origins of primary and secondary organic aerosol in Atlanta: Results of time-resolved measurements during the Atlanta Supersite Experiment. *Environ Sci Technol* 36(21):4489–4496.
24. Weber RJ, et al. (2007) A study of secondary organic aerosol formation in the anthropogenic-influenced southeastern United States. *J Geophys Res* 112(D13):D13302.
25. Hennigan CJ, Bergin MH, Russell AG, Nenes A, Weber RJ (2009) Gas/particle partitioning of water-soluble organic aerosol in Atlanta. *Atmos Chem Phys* 9(11):3613–3628.
26. Blanchard C, Hidy G, Tanenbaum S, Edgerton E (2011) NMOC, ozone, and organic aerosol in the southeastern United States, 1999-2007: 3. Origins of organic aerosol in Atlanta, Georgia, and surrounding areas. *Atmos Environ* 45(6):1291–1302.
27. Moore RH, Nenes A, Medina J (2010) Scanning Mobility CCN Analysis – a method for fast measurements of size-resolved CCN distributions and activation kinetics. *Aerosol Sci Technol* 44(10):861–871.
28. Parrish DD, et al. (2009) Overview of the Second Texas Air Quality Study (TexAQS II) and the Gulf of Mexico Atmospheric Composition and Climate Study (GoMACCS). *J Geophys Res* 114(D7):D00F13.
29. Russell M, Allen DT, Collins DR, Fraser MP (2004) Daily, seasonal, and spatial trends in $PM_{2.5}$ mass and composition in southeast Texas. *Aerosol Sci Technol* 38:14–26.
30. Bahreini R, et al. (2009) Organic aerosol formation in urban and industrial plumes near Houston and Dallas, Texas. *J Geophys Res* 114(D7):D00F16.
31. Lance S, et al. (2009) Cloud condensation nuclei activity, closure, and droplet growth kinetics of Houston aerosol during the Gulf of Mexico Atmospheric Composition and Climate Study (GoMACCS). *J Geophys Res* 114(D7):D00F15.
32. Wang J, Flagan RC, Seinfeld JH (2003) A differential mobility analyzer (DMA) system for submicron aerosol measurements at ambient relative humidity. *Aerosol Sci Tech* 37(1), 46–52.
33. Brock CA, et al. (2011) Characteristics, sources, and transport of aerosols measured in spring 2008 during the aerosol, radiation, and cloud processes affecting Arctic Climate (ARCPAC) Project. *Atmos Chem Phys* 11(6):2423–2453.
34. Mitchell J (1957) Visual range in the polar regions with particular reference to the Alaskan Arctic. *J Atmos Terr Phys* Special Supplement:195–211.
35. Rahn KA (1981) Relative importances of North America and Eurasia as sources of arctic aerosol. *Atmos Environ* 15(8):1447–1455.
36. Shaw GE (1995) The arctic haze phenomenon. *Bull Am Meteorol Soc* 76(12):2403–2413.
37. Warneke C, et al. (2009) Biomass burning in Siberia and Kazakhstan as an important source for haze over the Alaskan Arctic in April 2008. *Geophys Res Lett* 36(2):L02813.
38. Warneke C, et al. (2010) An important contribution to springtime Arctic aerosol from biomass burning in Russia. *J Geophys Res* 37(1):L01801.
39. Polissar A, et al. (1999) The aerosol at Barrow, Alaska: Long-term trends and source locations. *Atmos Environ* 33(16):2441–2458.
40. Matsui H, et al. (2011) Accumulation-mode aerosol number concentrations in the Arctic during the ARCTAS aircraft campaign: Long-range transport of polluted and clean air from the Asian continent. *J Geophys Res* 116(D20):D20217.
41. Moore RH, et al. (2011) Hygroscopicity and composition of Alaskan Arctic CCN during April 2008. *Atmos Chem Phys* 11(22):11807–11825.
42. Jacob DJ, et al. (2010) The Arctic Research of the Composition of the Troposphere from Aircraft and Satellites (ARCTAS) mission: Design, execution, and first results. *Atmos Chem Phys* 10(11):5191–5212.
43. Lathem TL, et al. (2012) Analysis of CCN activity of Arctic aerosol and Canadian biomass burning during summer 2008. *Atmos Chem Phys Discuss* 12(9):24677–24733.
44. Chow JC, et al. (1994) Temporal and spatial variations of $PM_{2.5}$ and PM_{10} aerosol in the Southern California air quality study. *Atmos Environ* 28(12):2061–2080.
45. Pastor SH, et al. (2003) Ambient single particle analysis in Riverside, California by aerosol time-of-flight mass spectrometry during the SCOS97-NARSTO. *Atmos Environ* 37:239–258.
46. Zhang Q, et al. (2007) Ubiquity and dominance of oxygenated species in organic aerosols in anthropogenically-influenced Northern Hemisphere midlatitudes. *Geophys Res Lett* 34(13):L13801.
47. Duong HT, et al. (2011) Water-soluble organic aerosol in the Los Angeles Basin and outflow regions: Airborne and ground measurements during the 2010 CalNex field campaign. *J Geophys Res* 116(D22):D00V04.

48. Moore RH, Cerully K, Bahreini R, Brock CA, Middlebrook AM, Nenes A (2012) Hygroscopicity and composition of California CCN during summer 2010. *J Geophys Res* 117(D7):D00V12.
49. Ensberg JJ, et al. (2012) Inorganic and black carbon aerosols in the Los Angeles Basin during CalNex. *J Geophys Res*, in press.
50. Moore RH, et al. (2012) CCN spectra, hygroscopicity, and droplet activation kinetics of secondary organic aerosol resulting from the 2010 Deepwater Horizon oil spill. *Environ Sci Technol* 46(6):3093–3100.
51. Bougiatioti A, et al. (2009) Cloud condensation nuclei measurements in the marine boundary layer of the Eastern Mediterranean: CCN closure and droplet growth kinetics. *Atmos Chem Phys* 9(18):7053–7066.
52. Bougiatioti A, et al. (2011) Size-resolved CCN distributions and activation kinetics of aged continental and marine aerosol. *Atmos Chem Phys* 11(16):8791–8808.
53. Engelhart GJ, Asa-Awuku A, Nenes A, Pandis SN (2008) CCN activity and droplet growth kinetics of fresh and aged monoterpene secondary organic aerosol. *Atmos Chem Phys* 8(14):3937–3949.
54. Engelhart GJ, Moore RH, Nenes A, Pandis SN (2011) Cloud condensation nuclei activity of isoprene secondary organic aerosol. *J Geophys Res* 116(D2):D02207.
55. Raatikainen T, Moore RH, Lathem TL, Nenes A (2012) A coupled observation-modeling approach for studying activation kinetics from measurements of CCN activity. *Atmos Chem Phys* 12(9):4227–4243.
56. Miles RE, Reid JP, Riipinen I (2012) Comparison of approaches for measuring the mass accommodation coefficient for the condensation of water and sensitivities to uncertainties in thermophysical properties. *J Phys Chem A* 116(44):10810–10825.
57. Padró LT, et al. (2012) Mixing state and compositional effects on CCN activity and droplet growth kinetics of size-resolved CCN in an urban environment. *Atmos Chem Phys* 12(21):10239–10255.
58. Asa-Awuku A, et al. (2011) (Airborne cloud condensation nuclei measurements during the 2006 Texas Air Quality Study. *J Geophys Res* 116(D11):D11201.
59. Ruehl CR, Chuang PY, Nenes A (2008) How quickly do cloud droplets form on atmospheric particles? *Atmos Chem Phys* 8(4):1043–1055.
60. Ruehl CR, Chuang PY, Nenes A (2009) Distinct CCN activation kinetics above the marine boundary layer along the California coast. *Geophys Res Lett* 36(15): L15814.
61. Asa-Awuku A, Engelhart GJ, Lee BH, Pandis SN, Nenes A (2009) Relating CCN activity, volatility, and droplet growth kinetics of β-caryophyllene secondary organic aerosol. *Atmos Chem Phys* 9(3):795–812.

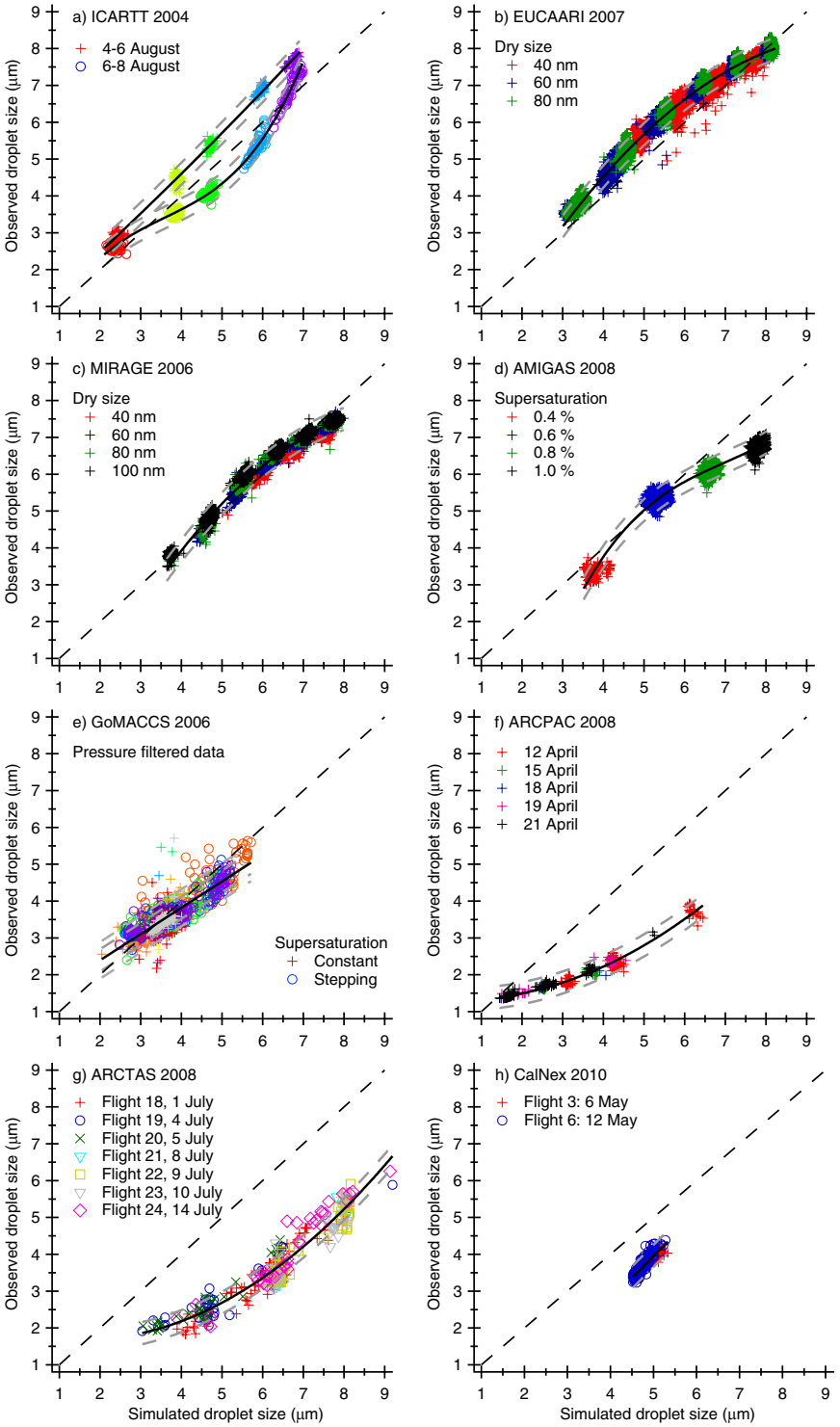

Fig. S1. Observed average droplet size as a function of simulated droplet size for the eight measurement campaigns. Each plot has a fitted solid line representing fast kinetics and the dashed gray lines represent ±0.3-μm uncertainty limits. Larger ±0.5-μm uncertainty limits are also shown for GoMACCS. The thin black dashed line shows the one-to-one correlation.

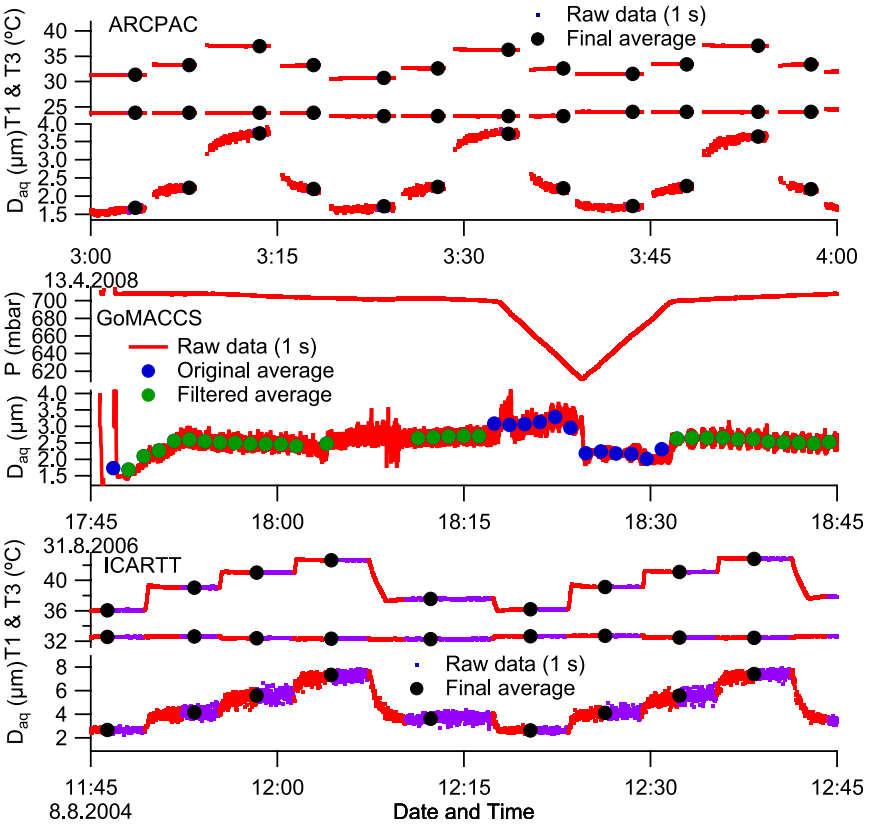

Fig. S2. Examples of filtering of data collected from three field campaigns.

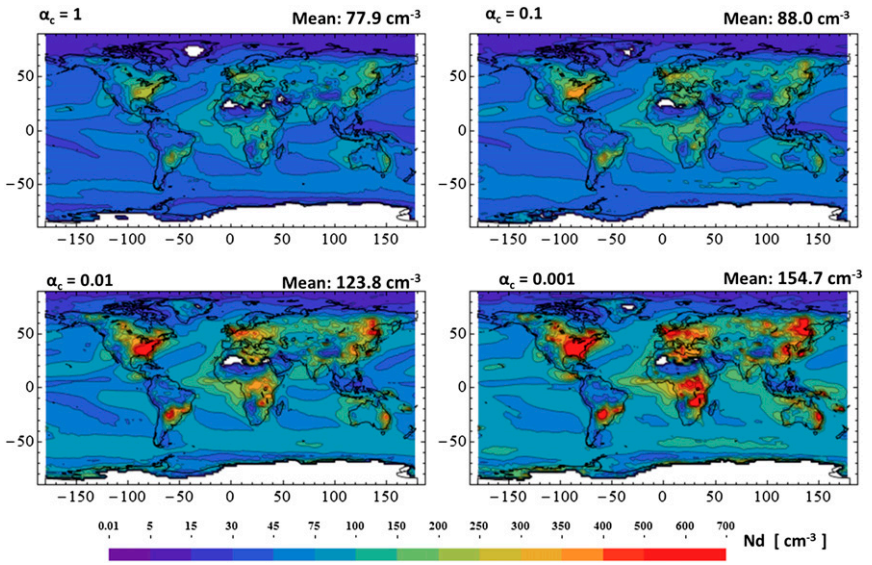

Fig. S3. Annual average cloud droplet number concentration for preindustrial emissions (936 mb pressure level). Number at the top right corner of each subplot represents the global annual average mean concentration. Results are shown for α_c = 1.0, 10^{-1}, 10^{-2}, and 10^{-3}.

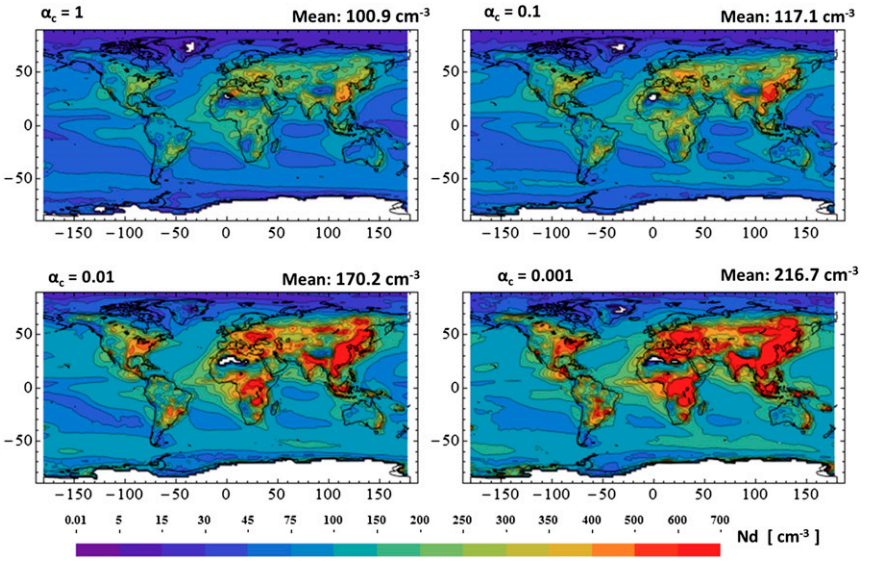

Fig. S4. Similar to Fig. S3 but for current day emissions.